CISTER

Journal Paper

Assessing Short-range Shore-to-Shore (S2S) and Shore-to-Vessel (S2V) WiFi Communications

Pedro d'Orey*

Miguel Gutiérrez Gaitán*

Pedro Miguel Santos*

Manuel Ribeiro

J. Borges de Sousa

Luís Almeida*

Assessing Short-range Shore-to-Shore (S2S) and Shore-to-Vessel (S2V) WiFi Communications

Pedro d'Orey*, Miguel Gutiérrez Gaitán*, Pedro Miguel Santos*, Manuel Ribeiro, J. Borges de Sousa, Luís Almeida*

*CISTER Research Centre

Rua Dr. António Bernardino de Almeida, 431

4200-072 Porto

Portugal

Tel.: +351.22.8340509, Fax: +351.22.8321159

E-mail: ore@isep.ipp.pt, mjggt@isep.ipp.pt, pss@isep.ipp.pt, maribeiro@fe.up.pt, jtasso@fe.up.pt, lda@fe.up.pt

https://www.cister-labs.pt

Abstract

Wireless communications increasingly enable ubiquitous connectivity for a large number of nodes, applications and scenarios. One of the less explored scenarios are aquatic ecosystems, specially when enabled by near-shore and short-range communications. Overwater communications are impaired by a number of distinguishing dynamic factors, such as tides, waves or node mobility, that lead to a widely fluctuating and unpredictable channel. In this work, we empirically characterize near-shore, overwater channels at 2.4 GHz under realistic conditions, including tidal variations, and relatively short TX-RX separations. To this end, we conducted experiments in a coastal estuarine region and on a harbor to characterize Shore-to-Shore (S2S) and Shore-to-Vessel (S2V) communication channels, respectively, and to identify major factors impairing communication in such scenarios. The empirical results show that constructive/destructive interference patterns, varying reflecting surface, and node mobility (i.e. travel direction and particular maneuvers) have a relevant and noticeable impact on the received signal strength. Thus, a set of parameters should be simultaneously considered for improving the performance of communication systems supporting S2S and S2V links, namely tidal variations, reflection surface changes, antenna height, TX-RX alignment and TX-RX separation. The results useful provide insights into realistic S2S and S2V link design and operation.

Assessing Short-range Shore-to-Shore (S2S) and Shore-to-Vessel (S2V) WiFi Communications

Pedro M. d'Orey [a,b,*], Miguel Gutiérrez Gaitán [c,a], Pedro M. Santos [a], Manuel Ribeiro [d], João Borges de Sousa [d,e], Luís Almeida [e,a]

[a] CISTER, Instituto Superior de Engenharia do Porto, IPP, Porto, Portugal
[b] Faculty of Sciences, University of Porto, Porto, Portugal
[c] Department of Electrical Engineering, Pontificia Universidad Católica de Chile, Santiago, Chile
[d] LSTS, Universidade do Porto, Porto, Portugal
[e] Faculty of Engineering, University of Porto, Porto, Portugal

A R T I C L E   I N F O

A B S T R A C T

Wireless communications increasingly enable ubiquitous connectivity for a large number of nodes, applications and scenarios. One of the less explored scenarios are aquatic ecosystems, specially when enabled by near-shore and short-range communications. Overwater communications are impaired by a number of *distinguishing* dynamic factors, such as tides, waves or node mobility, that lead to a widely fluctuating and unpredictable channel. In this work, we empirically characterize near-shore, overwater channels at 2.4 GHz under realistic conditions, including tidal variations, and relatively short TX-RX separations. To this end, we conducted experiments in a coastal estuarine region and on a harbor to characterize Shore-to-Shore (S2S) and Shore-to-Vessel (S2V) communication channels, respectively, and to identify major factors impairing communication in such scenarios. The empirical results show that constructive/destructive interference patterns, varying reflecting surface, and node mobility (i.e. travel direction and particular maneuvers) have a relevant and noticeable impact on the received signal strength. Thus, a set of parameters should be simultaneously considered for improving the performance of communication systems supporting S2S and S2V links, namely tidal variations, reflection surface changes, antenna height, TX-RX alignment and TX-RX separation. The results useful provide insights into realistic S2S and S2V link design and operation.

1. Introduction

Data communications and networking enable a wide range of human and industrial activities worldwide. Wireless communications, specifically, have developed remarkably over the last decades, not only because of their inherent flexibility but also due to their efficacy in progressively meeting the ever-increasing requirements of various applications. Technological developments have been made for improving energy efficiency [1], data rate [2], reliability [3], latency [4], mobility support, among many others. Wireless networks operate in an increasingly larger number of scenarios, ranging from cities [5] to deserts [6] or oceans [7]. On the other hand, networks should support massive node densities [8], often of highly mobile nodes. Thus, efficiently enabling ubiquitous connectivity for a large number of terminals, applications, and scenarios is increasingly important.

The Internet of Things (IoT) is a prime example of such advancements, especially in terrestrial environments. However, considerably less work has been done in aquatic environments (e.g. sea, lakes, rivers), despite the relevance of the related applications and use cases (e.g. for real-time vessel-to-shore video transmission [9] or aquaculture [10]). Communication patterns in water environments are diverse, namely in terms of node types, scenarios, requirements, or communication technologies. Three main communication regions are commonly considered [7]: near-shore, deep sea, and transoceanic. Besides (autonomous) aquatic nodes (e.g. autonomous underwater vehicles a.k.a. AUVs), maritime communications for IoT might include also aerial nodes (e.g. balloon, UAV), ground stations or even satellite communications for improved performance [11,12]. In this work, we focus on the less explored *near-shore* overwater communications, which is especially common and relevant in the so-called Maritime IoT.

Overwater (shore-based) communication is impaired by a number of dynamic factors, such as tides [13] or waves [7]. Tides lead to variable antenna heights causing varying interference patterns between direct

---

and (water) reflected paths resulting in considerable signal variations at the receiver. On the other hand, ocean dynamics (e.g. waves, wind, currents) can cause irregularities in the reflecting water surface leading to scattering and shadowing in agitated sea conditions [14], among other effects. In addition, links can be blocked by other (moving) objects (e.g. boats [15]) or infrastructure (e.g. buildings [16]). All these factors combined lead to widely fluctuating and unpredictable overwater links, which can affect the performance of wireless communication systems.

In this work, we seek to study and characterize overwater short-range communications, in both Shore-to-Shore (S2S) [e.g. environmental monitoring] and Shore-to-Vessel (S2V) communications [e.g. AUV data offloading], under realistic conditions (e.g. low antenna height and node mobility). Specifically, we consider near-shore communications over salty water influenced by tidal variations. We collected two large-scale datasets in (*i*) a coastal estuarine region for assessing S2S communications and (*ii*) a harbor for evaluating S2V communications using an AUV, both using commercial off-the-shelf (COTS) communication devices operating in the 2.4 GHz frequency band. Our main objective is to understand the influence of the tides and other dynamic factors (e.g. node mobility) on the large-scale signal propagation for short-range overwater links. The results shall provide insights into realistic link design and operation, e.g. to avoid the deep nulls (and poor channel features) that may occur along the tides. The main contributions of the paper can be summarized as follows:

- characterization of short-range overwater WiFi communications under realistic conditions (e.g. low AUV antenna heights);
- study the impact of dynamic factors, such as node mobility or tidal variations, on received signal strength;
- provision of publicly available datasets on S2S and S2V communications.

The remainder of the paper is organized as follows. The relevant related work is described in Section 2. Section 3 presents the experimental setup, evaluation methodology and the empirical characterization for S2S communications. Section 4 provides a similar description of S2V communications. The main results are further discussed in Section 5. The main conclusions and future work directions are given in Section 6.

2. Related work

Much work has been conducted within the broad area of maritime communications [17–20]. 5G [21,22], WiFi [23,24], LoRa [25, 26], ZigBee [27], among other technologies, have been considered to support wireless communications in water environments. Overwater communication involving onshore nodes is commonly separated into two categories given the different propagation characteristics and impairments:

- *Shore-to-Shore (S2S)* [13,23–25,28,29]
- *Shore-to-Vessel (S2V)* [29–32]

Communication links can be further characterized as *short-range* (e.g. [28]) or *long*-range (e.g. [24]) [i.e., several km], with the vast majority of the research focusing on the latter. For instance, prior work has been devoted to analyzing the impact of tidal fading [13], evaporation duct [33] or waves [7] on long-range signal propagation. A survey on the long-range outdoor WiFi networks can be found in [34]. We herein review relevant related research on S2S and S2V communications separately, giving special emphasis to short-range, WiFi and empirical evaluations given the nature of our study.

2.1. Shore-to-Shore (S2S)

Long-range S2S WiFi communication links have been reported in the literature as an alternative to providing high-bandwidth connectivity in remote regions separated by seawaters [23,24]. Short-range overwater WiFi communication is deemed as a more recent setup driven by emerging IoT-based communication scenarios at near-shore, especially when high-bandwidth requirements are posed. S2S overwater links at short to medium-range distances have also been considered in the past, often to support WSNs' infrastructure but typically using different communication technologies, e.g., ZigBee [27].

S2S short-range overwater communications for IoT are particularly affected by tides because changes in the water level can be in the order of antenna heights; which may intensify the impact of the constructive/destructive influence of surface reflections [35] (a.k.a., tidal fading). Experimental studies to characterize tidal impact in S2S WiFi short-range overwater links are restricted to few works [28,36], regardless of being a common propagation issue. Tidal fading [37] is, in fact, a detrimental phenomenon in overwater links, which despite efforts reported in a few recent works [13,25], remains still a barely explored condition. Some other works have evaluated related issues, e.g., the impact of the river level on large-scale fading of mixed water/land paths [38], the influence of antenna heights on links deployed over a small lake [28], the analysis of the water level impact on routing [14], and the use of different antenna polarization over tidal waters [35].

2.2. Shore-to-Vessel (S2V)

Wireless communication from shore to ships is commonly discussed in the literature of long-range maritime communications [17,18,32]. Surendran et al. [39] characterized S2V long-range (50+ km) marine wireless links, also analyzing factors influencing node connectivity, namely distance, wave-induced vessel motion and antenna orientation. Roux et al. [40] evaluated long-range maritime S2V radio links in the 3.5 and 5.8 GHz frequency bands demonstrating impairments to the propagation channel due to both masking effects from coastal relief and tides. Lee et al. [41] measured short to medium-range maritime S2V radio links operating at 2.4 GHz using antennas at conventional heights (4.5 m) showing that the two-ray model and Rician distribution characterize well large and small-scale fading. Reyes-Guerrero et al. [42] performed a buoy-to-ship channel measurement campaign in the 5.8 GHz frequency band exhibiting the difference between Line-of-Sight (LOS) and Non-LOS (NLOS) links.

While long-range overwater settings share several similarities with short-range configurations, short-distance overwater links using low (or very low) antenna heights pose different challenges to radio propagation. As in the S2S case, the impact of tides and waves can intensify signal degradation, which can get further aggravated in S2V scenarios, e.g. due to the influence of vessel mobility [43]. Despite this being a common situation in the emerging maritime IoT, few studies have characterized this impact in realistic IoT operation conditions, empirically.

S2V short-range WiFi communication is a relatively recent but common deployment scenario in IoT. Smart marinas, harbors, and other coastal locations are introducing the usage of autonomous vessels such as USVs or AUVs for different purposes, including seafloor mapping [44] and leak pipeline inspection [45], among others [9]. Despite this trend, efforts to characterize WiFi performance in these distinctive conditions are still not many [30,31,46], deserving further attention.

2.3. Discussion

While WiFi technology has a long-standing history in maritime communication, few research efforts have been made to characterize its large-scale signal behavior at *short-range*. The amount of literature is even less if considering this short-range WiFi communication occurs
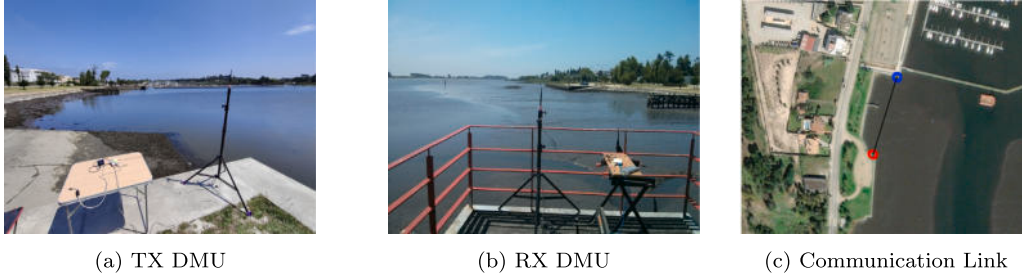
(a) TX DMU   (b) RX DMU   (c) Communication Link

Fig. 1. Experimental setup.

from the shore to communicate with autonomous vehicles such as USVs or AUVs operating at the surface, or in the form of shore-to-shore WiFi links supporting IoT monitoring applications over tidal waters. Both these cases are emerging but rather common scenarios that have been little explored in the literature, especially from an empirical characterization perspective. Detrimental issues such as tides, sea waves, and other water-level phenomena are often ignored in the empirical characterization of shore-to-X communications, especially when involving surface vehicles, buoys, or boats, which often rely on onshore connections. Moreover, while it has been demonstrated that, e.g., WiFi, can achieve kilometric distances over sea paths (see e.g., [13,24]), it is also known that this range can be severely reduced when antenna heights are at only a few meters from the water surface, due to reduced Fresnel zone clearance.

To the best of our knowledge, this research offers the first empirical assessment of S2S and S2V WiFi communication under key realistic conditions, namely (i) low antenna heights on shore, while operating at a very low antenna height on the vessel (AUV at the surface); and (ii) presence of dynamic factors such as node mobility, particularly vessel heading, and tides.

3. Evaluating Shore-to-Shore (S2S) communication

3.1. Experimental evaluation

3.1.1. Experimental setup

The experimental setup (Fig. 1) is composed of two static Dedicated Measurement Units (DMUs), namely a transmitter (TX) and a receiver (RX). Each DMU is equipped with three main components: (*i*) *GNSS device* with external antenna (Adafruit Ultimate GPS Breakout) for acquiring positioning and timing information, (*ii*) *IEEE 802.11 b/g/n radio* (Amiko WLN-880 with a Ralink RT5370 chipset) operating in the 2.4 GHz band equipped with external vertically positioned omnidirectional antennas with 5 dBi gain and (*iii*) Raspberry Pi single-board computer for data acquisition and storage. All radios were configured with the following settings: (i) channel 6 with center frequency 2437 MHz, (ii) 20 MHz bandwidth, and (iii) transmit power set to 30 dBm. The radios transmit standard compliant beacons every 102.4 ms in IEEE 802.1b mode with a data rate of 1 Mbps and length of 94 Bytes.

3.1.2. Experimental conditions

Measurement site. The measurement campaign was conducted in the northern part of the coastal lagoon-estuarine system of *Ria de Aveiro*, specifically, in Carregal, Ovar, Portugal, during May 2021. The communication links operated over an intertidal zone, which resulted in a varying reflecting surface from water to mud with different water content levels. The measurements were performed solely during the ebb period from approximately 10h21 until 13h06.

Installation. The TX was placed on-shore at (40.858485, −8.658307), while the RX was placed on a fenced pier at (40.859308, −8.657970) leading to a TX-RX separation of approximately 95.8 m. The DMU WiFi antenna was attached to an adjustable tripod. The distance between

the TX and RX DMU WiFi antenna base to the floor was approximately 156 and 122 cm, respectively. As both setups were installed on-shore, their antenna heights w.r.t. the water surface varied due to the tide as detailed in Section 3.2.2. All heights have been measured with a conventional tape with 0.1 cm precision.

Propagation Conditions. Transmitter and receiver were in Line of Sight (LoS) conditions being surrounded by several structures or objects (e.g. cars) that could cause reflections. The water was calm not causing shadowing or significant scattering [47]. We solely analyze TX to RX transmissions assuming link reciprocity [48]. Moreover, during the experiments, all nodes were kept static.

3.1.3. Measurement methodology

The RX radio was put in monitor mode, capturing all exchanged frames using the *tcpdump* application. Following, we processed the resulting file to obtain the current system unix timestamp (t^i_{system}) and the Received Signal Strength Indicator (RSSI). Positioning and timing information was acquired with a frequency of 1 Hz using a GPS receiver. To overcome clock drifts, measurements from different nodes were aligned using the current GPS time (t^i_{GPS}) that was stored together with the system UNIX timestamp to determine the current clock offset ($\Delta = t^i_{system} - t^i_{GPS}$).

3.2. Dataset characterization

3.2.1. System dynamics (traffic generation)

The TX radio was configured to transmit IEEE 802.11 beacons with a frequency of approximately 10 Hz (period of 102.4 ms) and a fixed frame size of 94 Bytes. However, the effective average period was approximately 141.96 ms due to channel scanning, which did not affect the validity of the results given the duration of the experiments. In total, approximately 70 k beacon frames were transmitted during the experiments.

Fig. 2 depicts the Cumulative Distribution Function (CDF) and the Probability Distribution Function (PDF) of the metric *Packet Inter-Reception time (PIR)*, i.e. time interval elapsed between the successful reception of two consecutive packets. The inter-reception time is below 105.72 ms for 90% of the cases. As expected, the data exhibits spikes in multiples of the defined beacon interval of 102.4 ms, existing an exponential decay of the probability for increasing beacon intervals.
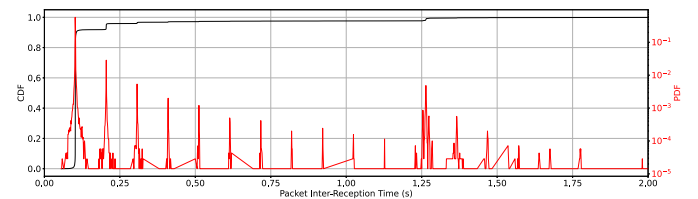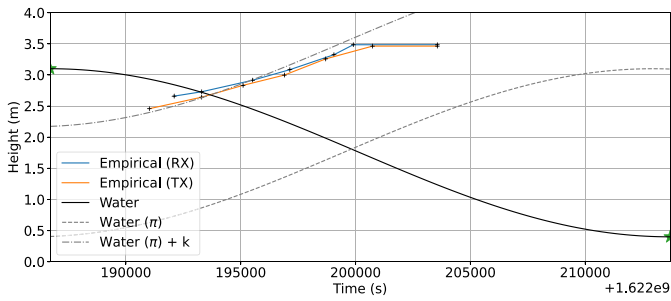

Fig. 2. Traffic generation using PIR metric.

Fig. 3. Tide-induced water level variations (S2S). The *x*-axis represents the Unix epoch, i.e. the number of seconds elapsed since January 1, 1970, 00:00:00 UTC. (For interpretation of the references to color in this figure legend, the reader is referred to the web version of this article.)

Consecutive packet losses lead to increasing PIR values; the probability of having *n* consecutive packet losses decreases for increasing *n*. This pattern does not hold for PIR values slightly above 1228.8 ms (i.e. 12 beacon intervals) – as explained previously – due to the channel scanning performed by the network card over 11 WiFi channels in the 2.4 GHz frequency band. In general, the spread around the spike decreases for larger PIR values.

3.2.2. Environmental dynamics

The antenna heights with respect to the water surface varied during the experiments due to the recurrent rise and fall of the water level (i.e. tides). In fact, the sea level in large bodies of water is determined in great measure by the varying gravitational forces of both the Moon and the Sun, and the rotation of the Earth [49]. Moreover, tides are also influenced by astronomical (e.g. lunar orbit) and meteorological factors (e.g. wind). Water levels in open waters are typically described by a linear combination of sinusoidal terms.

Tidal data is publicly available through a number of sources (e.g. http://www.tabuademares.com). Fig. 3 depicts the predicted water level variations for the measurement site (Carregal, Portugal) during the ebb period of a semi-diurnal tide. The ebb period is defined as the period from high tide to low tide during which the water level is decreasing. The water level at high and low tides obtained from the publicly available dataset is approximately 3 m and 0.5 m, respectively [represented by the green stars]. The water level varies by more than 2.5 m during this period of approximately 7 h and 30 min. We approximate tidal dynamics using a simple sinusoidal model [in black] and plot the same data with a phase shift of π [in dashed gray] for comparison with empirical data.

The empirical measurements of the effective TX and RX antenna heights w.r.t. the current water level are also depicted [in orange and blue, respectively]. Since the experiments were carried out during the ebb period, the antenna heights increase by about 1 m reaching a maximum of approximately 3.5 m when the reflecting surface changes from water to lagoon bottom. For simplicity reasons, we consider the bottom (made of mud) as a flat surface when calculating the antenna heights. During the measurement campaign, the reflection point was always on a fairly flat surface, either water or mud. However, if the reflection point moves on a non-flat surface due to asymmetries in the antenna heights, bathymetric data can be used to track the actual heights with respect to the reflection point (e.g. see [25]) and thus beyond the scope of our study. Comparing the empirical (transmitter antenna height) measurements and the adjusted output of the tidal model [dashed-dotted gray line], we observe well-aligned trends, demonstrating the feasibility to model the phenomena with small error magnitudes, just using an offset k ($\approx$1.7684 m) for the transmitter. Previous work [31] has shown that centimeter-level differences in antenna height can have a significant impact on the channel characteristics.
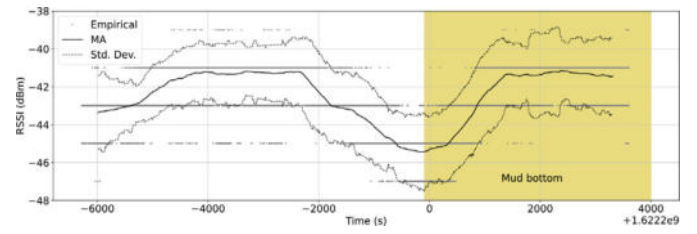

Fig. 4. RSSI variations as a function of time represented using the Unix epoch (S2S).
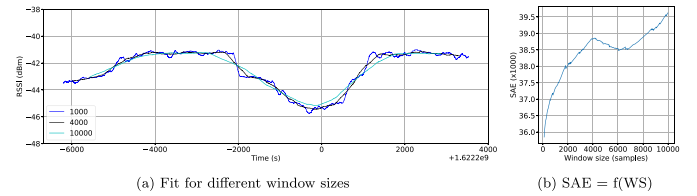

(a) Fit for different window sizes   (b) SAE = f(WS)

Fig. 5. Selection of appropriate window size (S2S).

3.3. Results

We aim at characterizing large-scale signal fluctuations of S2S communication links operating over tidal zones. With this goal, we characterize signal variations using the Received Signal Strength Indicator (RSSI) and the system performance using the Packet Delivery Ratio (PDR).

Received Signal Strength Indicator (RSSI). Fig. 4 depicts the empirical RSSI measurements as a function of the time (*gray*) alongside the result of applying the moving average method with a window size of 4000 samples (*black*) and the corresponding upper and lower standard deviation bounds. For a given time instant, the mean is calculated resorting to the 2000 previous and the 2000 posterior samples (i.e. the window is centered around the current time instant). This window size was selected to achieve a good trade-off between accurately representing the underlying empirical data and smoothing the data to remove instantaneous fluctuations due to small-scale fading and noise (see Fig. 5(a)). The selection was made using the elbow method in the graph of the sum of absolute errors (SAE) as a function of the window size (Fig. 5(b)). This window size is much smaller than the rate of change of the water level, which is the primary factor for large-scale signal variations arising from varying antenna heights.

The effective antenna heights increase due to the falling tide during the ebb period until the lagoon bottom is exposed (around 12 h). After this time instant, the effective antenna heights remain constant. As the TX-RX separation remains constant, the increase of the effective antenna heights leads to variations in the received signal strength mainly arising from the constructive/destructive interference between the LOS and (water-)reflected paths that have different lengths. These constructive/destructive interference patterns are often modeled using the two-ray propagation model [28,50]. For more details on the two-ray propagation model we refer the reader to [51].

Due to ebb currents, the reflection surface changes from water to mud after a given time instant. Fig. 4 highlights (in yellow) the time window when the mud bottom becomes exposed. In this time period, the received signal strength varies up to 4 dB despite the antenna heights at the reflection point[1] being fairly constant. One possible explanation for these signal variations – that we shall further explore

---

[1] The reflection point is defined as the distance with respect to the receiver side at which the second ray touches the reflective (flat) surface.
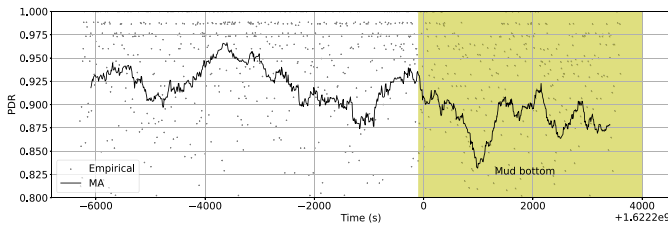
Fig. 6. PDR variations as a function of time represented using the Unix epoch (S2S). The gray dots represent empirical PDR measurements for a time interval of 10 s and the black curve is an approximation obtained using a moving average window technique.

Table 1
COTS hardware used in the S2V experiments.

Node	GNSS device	802.11 radio	Ant. Gain
AUV	Ublox EVK-6	Ubiquity Picostation M2	5 dBi
AP	Ublox EVK-6	Ubiquity Bullet M2	8 dBi
DMU	Adafruit Ultimate GPS Breakout v3	Amiko WLN-880	5 dBi

– might lie on the variation of the water content in the mud due to evaporation.

Packet Delivery Ratio (PDR). Fig. 6 depicts the PDR as a function of time. The PDR is defined as the ratio of delivered packets to the number of transmitted packets over a given time or distance interval. As the packet sequence numbers have not been stored, we approximate the PDR using the PIR metric for determining the number of consecutive packet losses, i.e. divide the PIR by the beacon interval of 102.4 ms. Furthermore, we filter PIR larger than 12 beacon intervals due to channel scanning issues. The results show that the PDR remains fairly constant at around 0.9 with a positive or negative magnitude of 0.05.

4. Evaluating Shore-to-Vessel (S2V) communication

4.1. Experimental evaluation

4.1.1. Experimental setup

The experimental setup (Fig. 7) is composed of three main nodes that exchange/acquire mission information (e.g. telemetry, controls), namely (*i*) Commercial Autonomous Underwater Vehicle (AUV) *Xplore-4*[2] [2 m long], (*ii*) WiFi Access Point (AP) termed *Manta*, and (*iii*) Dedicated Measurement equipment (DMU) [described in more detail in Section 3.1.1]. In manual mode, the AUV was operated by a Remote Vehicle Controller (RVC) associated with the AP at the beginning of the experiments.

Each node is equipped with two main components: (a) *GNSS device* with an external antenna for acquiring positioning and timing information and (b) *IEEE 802.11 b/g/n radio* operating in the 2.4 GHz band

equipped with external omnidirectional antennas with different gains. Table 1 presents a summary of the specific COTS equipment used in the experiments. The AP antenna was secured to the computing device case, while the DMU antenna was attached to the top of an adjustable tripod. To assess the impact of different onshore antenna heights on the overall system performance, the tripod height was set to the maximum and minimum positions constituting the termed *Experiment I* [Fig. 7(a)] and *Experiment II* [Fig. 7(b)] configurations, respectively. All radios were configured with the following settings: (i) channel 3 with center frequency 2422 MHz, (ii) 20 MHz bandwidth, and (iii) variable data rate. The AUV and AP transmit power have been set to 28 dBm and 25 dBm, respectively. The radios transmit mission-related data with varying frequencies, frame sizes, and bit rates.

4.1.2. Experimental conditions

Measurement site. The measurement campaign was conducted in the Port of Leixões, Matosinhos, Portugal, in July 2021. The port is located on the shore of the North Atlantic Ocean behind a coastal breakwater, thus still existing water level variations induced by tides. The measurements were performed solely during the flooding period. The duration of experiments I and II was 28.5 min and 26.4 min comprising 7 and 6 complete round-trip missions, respectively.

Installation. The AP and DMU nodes were placed on a concrete pier of the harbor at (41.185246, −8.704901) and (41.185273, −8.704882), respectively. The AUV operated in an enclosed area of the port. The distance between the AP and DMU WiFi antenna base to the pier floor was 0.37 m, and 3.55/1.15 m for experiments I/II, respectively. The heights have been measured with a conventional tape with 0.1 cm precision. The AP and DMU were installed on-shore, thus their antenna heights w.r.t. the water surface varied due to the tide. The AUV antenna height w.r.t. the water was 17 cm. The distance between the first floating element of the front/back of the AUV and its WiFi antenna is 127.5 cm and 33.5 cm, respectively.

AUV Mobility. The AUV was set to operate autonomously following a predetermined path defined by a set of waypoints. For safety reasons,

---

[2] https://www.oceanscan-mst.com/.
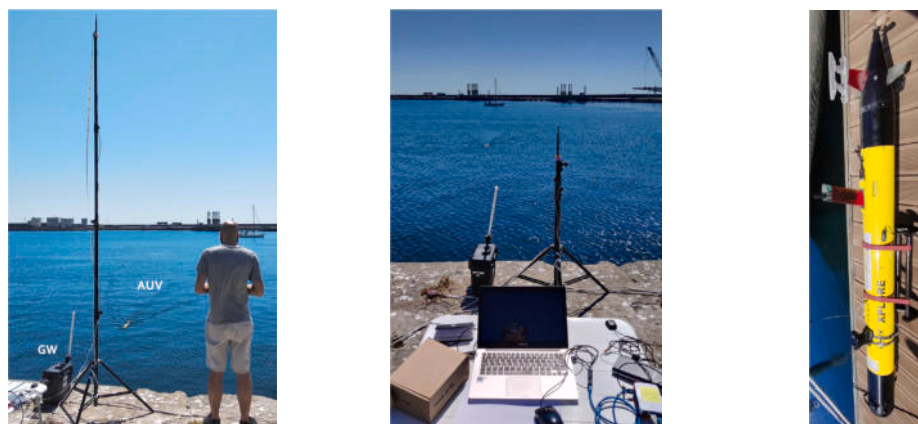
(a) Onshore setup (higher DMU antenna height for Exp. I).

(b) Onshore setup (lower DMU antenna height for Exp. II).

(c) Autonomous Underwater Vehicle (AUV) *Xplore-4*

Fig. 7. S2V Experimental setup.

(a) AUV trajectory (in blue) and (mean) AP/DMU GPS positions. Reference COG values are depicted in the upper right corner.

(b) Distance between AUV and AP/DMU for Exp. I (red area) with 7 round trips and Exp. II (blue area) with 6 round trips.
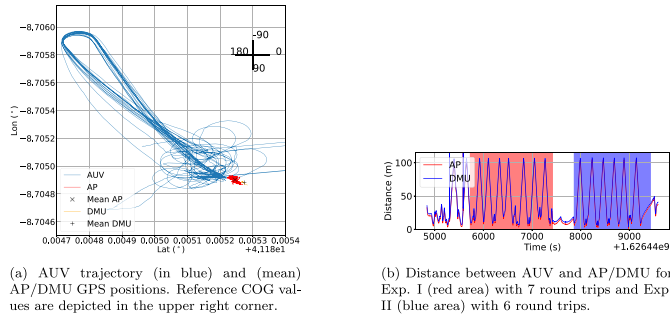
Fig. 8. Node locations and AUV mobility patterns. (For interpretation of the references to color in this figure legend, the reader is referred to the web version of this article.)

(a) Inter-Reception Time

(b) Frame Size

Fig. 9. Traffic generation statistics.

(a) COG

(b) Speed

(c) Horizontal DOP

Fig. 10. Mobility data analysis, namely Course of Ground (COG), Speed and Horizontal Dilution of Precision (HDOP).

the AUV was controlled manually near the quay. Fig. 8(a) shows the AUV trajectory (in blue) and the mean GPS positions of the AP and DMU. The AUV performed 13 equivalent round-trip missions starting from the quay and moving until ∼100 m away (Fig. 8(b)), with Exp. I and Exp. II consisting of 7 and 6 round-trip missions, respectively. The AUV operated always on the surface at a low speed (1 m/s).

Propagation Conditions. Transmitter and receiver were predominantly in Line of Sight (LoS) conditions, except for rare occlusions caused by the quay and surrounding boats. The water was calm not causing shadowing or significant scattering [47]. We solely analyze AUV to AP/DMU transmissions assuming link reciprocity [48].

4.1.3. Measurement methodology

The AUV and AP devices measured the received signal strength with a 1 Hz rate using the manufacturer's software. On the other hand, to improve temporal resolution, the DMU radio was put in monitor mode, capturing all exchanged frames using the *tcpdump* application. Following, we processed the resulting file to extract: (i) current system unix timestamp (t^i_{system}), (ii) frame identifier, (iii) frame (sub-)type, (iv) frame length, (v) TX's MAC address, (vi) Received Signal Strength Indicator (RSSI) and (vii) data rate.

Positioning and timing information was acquired with a frequency of 1 Hz. To overcome clock drifts, measurements from different nodes were aligned using the current GPS time (t^i_{GPS}) that was stored in a separate file along with the current node position and the system UNIX timestamp to determine the current clock offset ($\Delta = t^i_{system} - t^i_{GPS}$). The TX-RX node separation (distance) was determined by combining positioning and timing data and associated to the performance data (i.e. RSSI).

To study the influence of AUV mobility, we split manually the data into two types of segments using the TX-RX separation and AUV heading and velocity: (i) *approach* (i.e. AUV approaching shore node) and (ii) *recede* (i.e. AUV moving away from shore node).

4.2. Dataset characterization

4.2.1. System dynamics

Traffic generation. The AUV repeatedly executed its mission in the defined area moving perpendicular to the quay, maintaining its usual operational communication pattern, i.e., exchanging with the AP several types of data related to each of its sub-systems (e.g. networking, maneuvering or vehicle supervision). Due to differences in the underlying processes, the message generation frequency and packet sizes are distinct for different message types. In total, ∼240 k/228 k frames were transmitted by the AUV (15.5/15.1% of all exchanged frames) during experiments I and II, respectively.

Since the traffic generated by the AUV was not logged, we approximate the traffic rate using the Packet Inter-Reception time (PIR) metric.
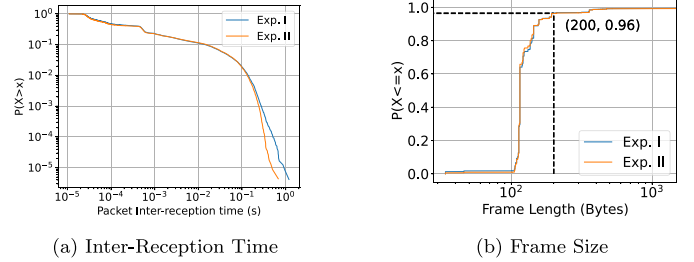
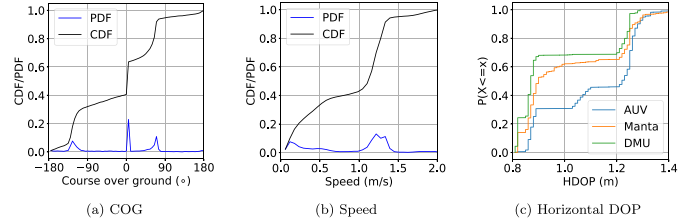Fig. 9(a) presents the inverse CDF of the PIR metric for Exp. I and II. The analysis shows that the PIR is below 10 ms in 90% of the cases, enabling also a fine-grained tracking of received signal power in time. The analysis also shows very similar PIR distributions for the two experiments, except for the larger tail in Exp. I for PIRs larger than 0.2 s. Fig. 9(b) shows the CDF of the frame size revealing a relatively small frame with similar distributions for Exp. I and II. In particular, ∼96% of the frames are less than 200 Bytes long.

Mobility data. Fig. 10 shows an analysis of the AUV mobility resorting to the COG, speed and HDOP metrics. The *Course of Ground* (*COG*) describes the actual direction of travel of the (autonomous) vehicle. Fig. 10(a) show that the range of COG angles is not equally sampled and that there exist three main travel directions, i.e. approximately {−125°, 5°, 70°}. The unequal sampling of the COG range arises from the (i) manual maneuvering of the AUV when in proximity to the quay and (ii) the initial objective of the experiments, which was to assess the impact of different onshore antenna heights on the performance of the communication link. Fig. 10(b) depicts the CDF and PDF of the AUV speed, with the main mode of the distribution being slightly above the defined mission speed of 1 m/s due to water currents.

Nodes resort to GPS receivers to acquire position and time, which in turn is used to compute the distance between AUV and onshore nodes. For obtaining reliable (link quality) results, the precision of positioning data should be high. Fig. 10(c) presents one of the most popular positioning precision metrics termed Horizontal Dilution of Precision (HDOP), which quantifies the effect of satellite-user geometry (i.e. the positions of the satellites relative to the user) on horizontal position accuracy [52]. A lower HDOP value indicates a better horizontal position accuracy. The results show that for all setups the HDOP varies between 0.8 and approximately 1.4 m, which are within typical values (e.g. see [53,54]) and considered acceptable given the low vehicle speed (≈1.25 m/s) and that typical bin sizes for link quality evaluations are larger than 10 m (e.g. 25 m in [55] and 20 m in [56]). As expected, the HDOP value is higher for the mobile AUV. Due to favorable conditions (e.g. open sky), all setups have on average 10 visible satellites (well distributed around the user), which explains the low HDOP.

4.2.2. Environmental dynamics

Fig. 11(a) shows publicly available tidal data describing water level variations for the measurement site on July 16, 2021 during the flood
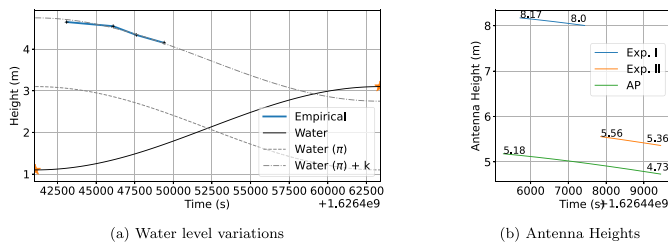
(a) Water level variations

(b) Antenna Heights

Fig. 11. Tide-induced water level variations (S2V). The *x*-axis represents the Unix epoch, i.e. the number of seconds elapsed since January 1, 1970, 00:00:00 UTC. (For interpretation of the references to color in this figure legend, the reader is referred to the web version of this article.)

period of a semi-diurnal tide. The flood period is defined as the period from low tide to high tide during which the water level is increasing. The water level at low and high tides obtained from the publicly available dataset is approximately 1.1 and 3.1 m, respectively [represented by the orange stars]. The water level varies by ∼2 m during this period of approximately 6 h. As for the S2S case, we approximate the tidal dynamics resorting to a simple sinusoidal model [in black] and plot the same data with a phase shift of π [in dashed gray] for comparison with empirical data of the distance between the pier floor and the current water level [in blue]. This height decreases during the experiments due to the rise of the water level during the flooding period of the tidal cycle. Again, we observe very well-aligned trends between the empirical (transmitter antenna height) measurements [in blue] and the adjusted output (offset $k \approx 1.645$ m) of the tidal model [dashed-dotted gray line]. Fig. 11(b) shows the antenna heights w.r.t. the water surface during the measurement campaign. The AP antenna height varied within [5.18, 4.73] m (45 cm). The DMU antenna height varied within [8.17, 8.0] m (17 cm) and within [5.56, 5.36] m (20 cm) for Exp. I and II, respectively. Despite both experiments having similar duration, the water level variations are slightly more pronounced in Exp. II due to higher flooding velocities in that part of the tidal cycle.

4.3. Results

In this work, we aim at characterizing large-scale signal fluctuations of shore-to-vessel communication links under realistic AUV/ASV mobility. Furthermore, we aim at assessing how the system performance is dynamically impaired by the node mobility, surrounding propagation environment, and TX-RX alignment.

4.3.1. Aggregated results

Fig. 12 depicts the RSSI as a function of the TX-RX separation for the three cases (AP, DMU exp. I and DMU exp II). For all cases (Fig. 12(a)), as expected, the RSSI decreases *non-monotonically* with increasing distance, with observable dips in received power for certain relatively short TX-RX separations (*interference region*) but becoming monotonic after the *break-point distance*[3] (*monotonic region*). For instance, the received power diminishes by almost 10 dB for a TX-RX separation of approximately 17 m for the AP setup; note that the magnitude of the drop is not so pronounced for the DMU setup. These variations in received signal strength mainly arise from the constructive or destructive interference between the LOS and water-reflected paths that have different lengths. These constructive/destructive interference patterns are often modeled using the two-ray propagation model [28, 50]. The raw RSSI data presented in Figs. 12(b) and 12(c)–12(d) makes

---

[3] In radio signal propagation, the break-point distance is commonly defined as the critical point where the path loss exponent (*n*) changes from one operation mode to another. For the two-ray model, this point typically refers to when *n* raises from 2 to 4 [57].

these sudden signal variations even more evident. As expected, the number and location of these dips vary for different configurations due to different antenna heights w.r.t. the water surface, which changes the path length for the water-reflected ray and consequently creates different interference patterns.

To analyze the variability of the RSSI for a given TX-RX separation bin, we resort to the average and the bounds of the standard deviation metric. The average standard deviation for all bins is 3.024, 2.374, and 2.309 for the AP, DMU exp. I and DMU exp. II setups, respectively. On the other hand, the minimum and maximum RSSI standard deviation values considering all bins are [0.408, 9.033], [1.139, 5.934], and [1.079, 6.317] for the same three cases, respectively. The results show that the (*i*) AP setup exhibits larger received signal variations (e.g. due to more pronounced null) and (*ii*) variations for the experiments I and II of *DMU* setup are similar.

Impact of Antenna Heights. In the deployment of shore-to-vessel communication systems, the common practice is to install onshore node antennas at the highest position the setup allows. In our experiments, we accommodate three antenna height ranges (Fig. 11(b)) to represent different settings. For the DMU setup, the results in Fig. 12(a) provide initial evidence that the highest antenna position often fails in providing the best link quality, as alluded in previous studies [28,58]. Note also the overlap between the shaded areas for experiments I and II. We argue that this occurs for several reasons, namely the (*i*) low AUV antenna height and (*ii*) short TX-RX distances (often falling within the self-interference zone), which can be explained by the geometrical basis of the two-ray model. For shorter TX-RX separations, the signal fluctuations are typically induced by the constructive and destructive interference between multiple propagation paths that reach the receiver with different phases arising from the existing TX-RX geometric configuration. Thus, in the so-called self-interference zone, higher antenna heights resulting in a given TX-RX geometric configuration (and thus interference pattern) do not necessarily lead to better link quality.

4.3.2. Impact of travel direction

To understand the influence of the AUV travel direction w.r.t. to the shore, we classified the collected data into *approach* and *recede* travel directions. For a fair comparison, we solely consider the data segments where the vehicle was operating autonomously.

Fig. 13 shows the RSSI as a function of distance split per travel direction. As expected, the RSSI as a function of the TX-RX separation (Fig. 13(a)) shows similar trends to the ones given in Fig. 12(a). Now comparing these trends for a given setup (e.g. Fig. 13(b) or 13(c) or 13(c)), we observe (substantial) differences between both travel directions in terms of magnitude and location of the dips. These differences are especially evident for the *AP* setup. While in the *AP* setup the *recede* direction shows higher RSSI (Fig. 14(a)), the received signal level is larger for the *approach* direction in the *DMU exp. II* setup (Fig. 14(c)). In the *DMU exp. I* setup the distributions of the RSSI for both travel directions are similar. In this context, we apply the Cramér–von Mises test [59] to statistically compare the distributions of the two directions in each setup considering a significance level of 5%. The null hypothesis for this criterion states the equality of distributions, i.e., observed samples are drawn from the same distribution. The results given in Table 2 show that the null hypothesis can only be rejected for the *AP* setup, i.e., samples are not drawn from the same distribution.

Several reasons can cause discrepancies between *approach* and *recede* communication links, namely (*i*) non-uniform radiation pattern of the quasi omnidirectional antennas, (*ii*) antenna tilting causing different TX-RX alignment due to the tilting of the AUV arising from its propulsion, among others.

Impact of Antenna Heights. For the DMU setup, the results corroborate previous findings that provide similar results in terms of RSSI for both travel directions despite the different antenna heights of Exp. I and II.
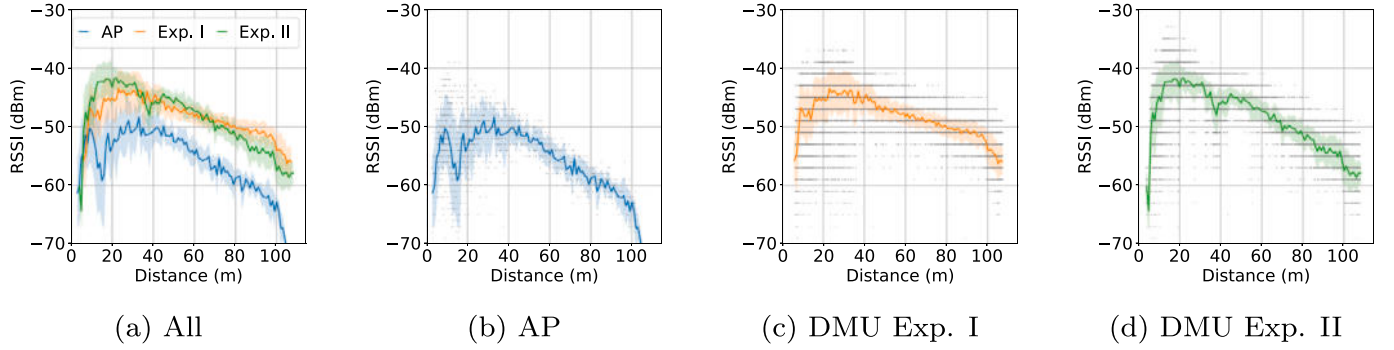
Fig. 12. RSSI as a function of TX-RX separation. Each tendency line [shaded area] is the mean RSSI [standard deviation above/below the mean RSSI] for the given distance bin. The points in (b), (c), and (d) represent raw RSSI measurements for the AP and DMU experiments I and II, respectively.
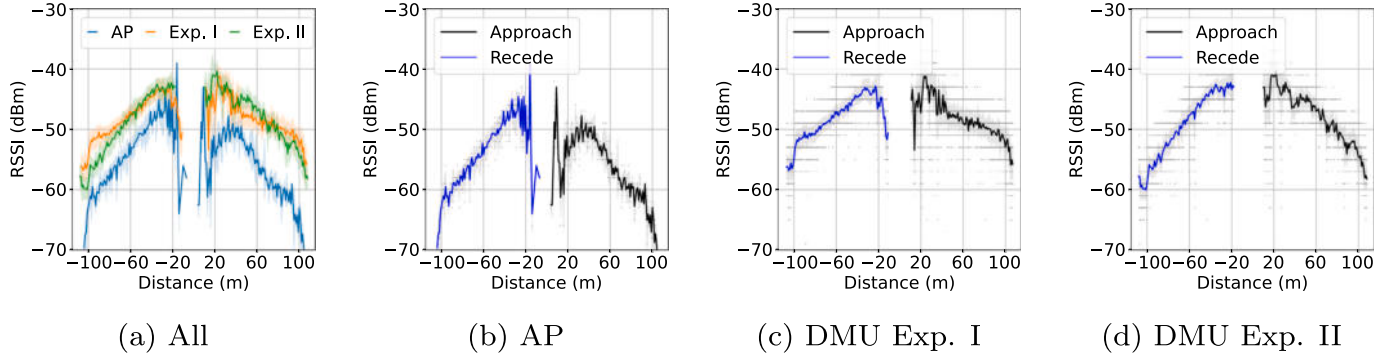

Fig. 13. RSSI for *approach* and *recede* travel directions. Each tendency line [shaded area] in (a), (b), (c) and (d) is the mean RSSI [standard deviation above/below the mean RSSI] for the given distance bin and travel direction. The points in (b), (c) and (d) represent raw RSSI measurements for each configuration.
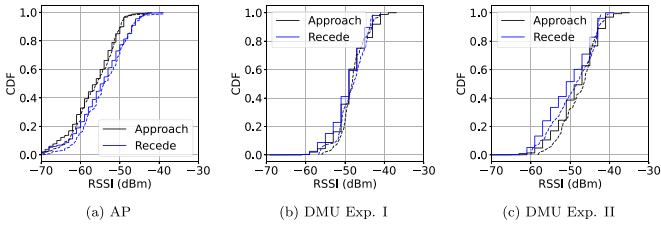

Fig. 14. RSSI CDF of the raw (full line) and aggregated (dashed line) data for the three configurations.

Table 2
Cramér–von Mises test between travel directions using aggregated data considering a significance level of 0.05.

Setup	Statistic	p-value	Result
AP	0.78323	0.00799	Reject
DMU Exp. I	0.24500	0.19578	Not reject
DMU EXp. II	0.39260	0.07571	Not reject

4.3.3. Impact of node mobility

Fig. 15 shows raw and aggregated RSSI as a function of time for DMU Exp. I[4] alongside mobility-related metrics, namely TX-RX separation, AUV speed and Course over Ground (COG). These results exhibit a clear impact of the AUV mobility pattern on the received signal strength. Specifically, despite the use of omnidirectional antennas and for similar TX-RX separations, (fast) AUV turns (shown by the COG metric) lead to clearer dips in the RSSI pattern. These dips, which can

---

[4] We omit the results for other configurations due to space constraints.

impair communication between the AUV and the shore node (e.g. link break or modulation adaptation), can be larger than 20 dB and are especially evident when the vehicle was being operated manually, i.e. outside the orange and blue bands corresponding to autonomous operation for the *recede* and *approach* travel directions, respectively.

Under autonomous operation, RSSI dips (not explained by destructive interference) occur also when the vehicle COG is approximately zero, i.e. the AUV is perpendicular to the shore node. Nevertheless, these dips are less pronounced when compared to the ones occurring during manual operation. We argue that this type of RSSI dips are due to TX-RX antenna misalignment that cause a degradation of transmitted/received signal given non-isotropic features in radiation patterns of these nodes; other effects (e.g. AUV structure) might also influence the effective radiation patterns.

Sudden signal variations are also observed at the end of the *approach* travel direction despite the constant AUV COG. We argue that this effect might be attributed to a change in the reflection surface of the secondary ray. The bottom image of Fig. 15 depicts the position of the reflection point w.r.t. to the AUV WiFi antenna. The results show that the reflection point lies within 2 m of the WiFi antenna. While for the majority of the *approach* and *recede* travel directions the reflection point lies in the water close to the AUV, extreme cases for the *approach* direction, only, may place the reflection point on the AUV body itself. Note that the WiFi antenna is placed towards the back part of the AUV as shown in Fig. 7(c), thus it does not affect the *receding* direction. Please recall that the distance between the first floating element of the front/back of the AUV and its WiFi antenna is 127.5 cm and 33.5 cm, respectively. The different characteristics of the materials that reflect the secondary ray (i.e. water and metallic AUV) will lead to changes in the reflection coefficient and consequently in the destructive/constructive interference pattern.
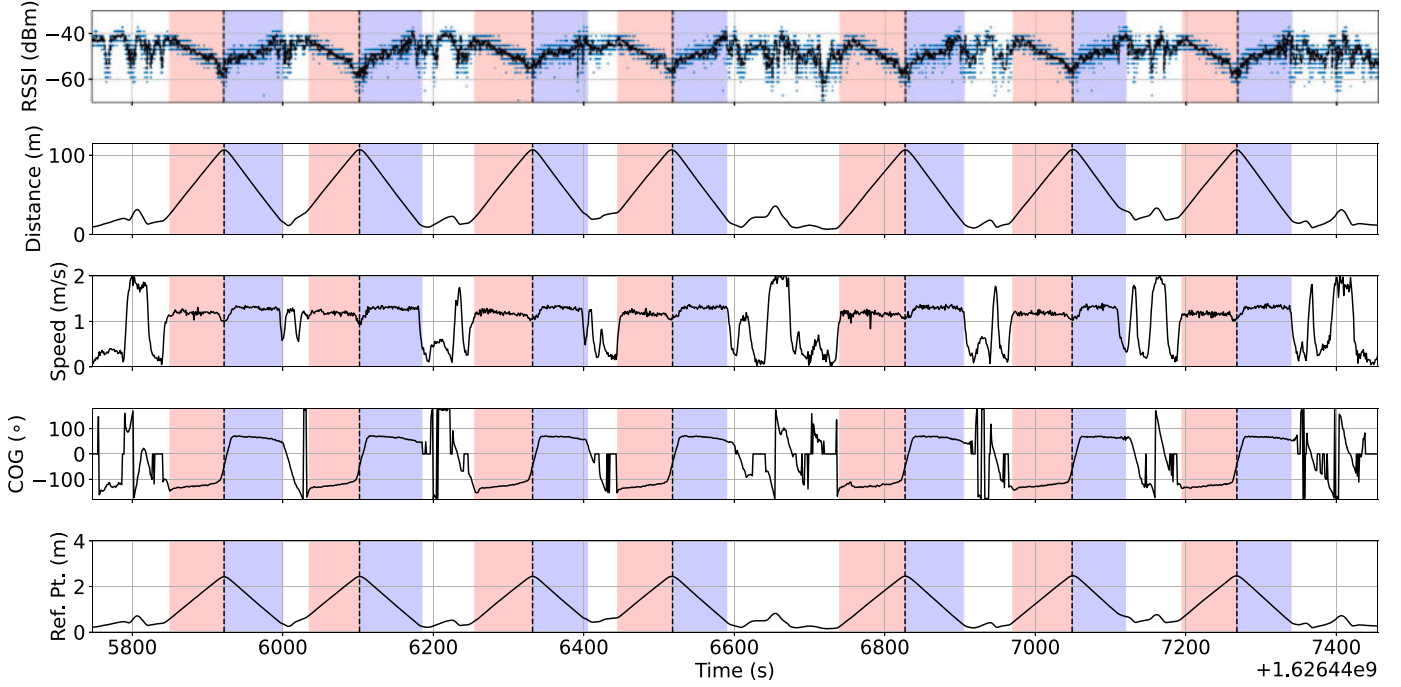
Fig. 15. Aggregated and raw RSSI as a function of time represented using the Unix epoch for DMU Exp. I, including temporal variation of the AUV-shore distance, AUV speed, Course over Ground, and reflection point distance w.r.t. AUV WiFi antenna. The segments corresponding to the *recede/approach* travel directions are depicted as orange/blue bands. (For interpretation of the references to color in this figure legend, the reader is referred to the web version of this article.)
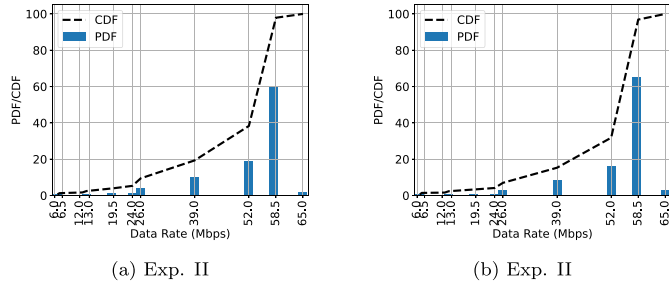

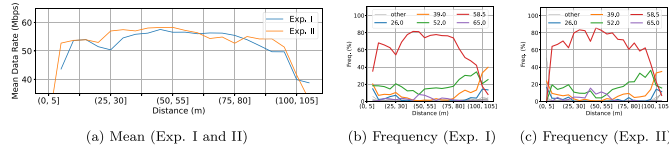**Fig. 16.** Frequency of negotiated IEEE 802.11 b/g/n data rates for experiments I and II.

Fig. 17. Negotiated data rates as a function of distance for experiments I and II. We consider a bin size of 5 m.

Fig. 18. Relative frequency of negotiated data rates as a function of the RSSI for experiments I and II. We consider a bin size of 2 dB.

4.3.4. Impact on data rate

To determine the instantaneous channel capacity, we extract the negotiated IEEE 802.11 data rate from each frame contained in the experimental packet capture files of experiments I and II. Note that the devices implemented a proprietary rate adaptation scheme [60]. Considering a bandwidth of 20 MHz and a single spatial stream, the data rates of an IEEE 802.11 b/g/n network vary between 1 Mbps and 65 Mbps using different modulation types and coding schemes. Fig. 16 depicts the relative frequency of each data rate for experiments I and II. For both experiments, the results demonstrate that the data rates are equal or larger than 26 Mbps in about 95% of the occasions given the favorable propagation conditions (e.g. LoS, no obstacles), with the most
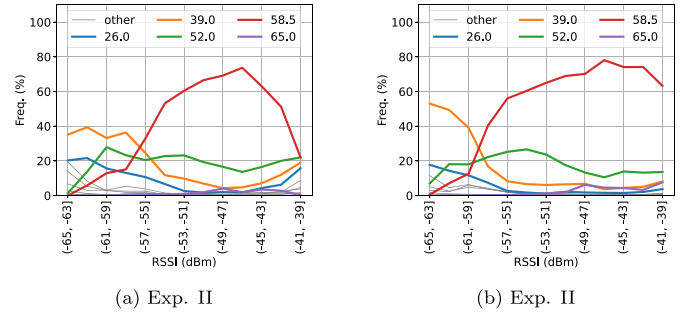
frequent data rate being 58.5 Mbps. As expected, the distributions of the data rates for experiments I and II are similar given the comparable conditions (e.g. in terms of RSSI as shown in Section 4.3.1).

Fig. 17 depicts the negotiated data rates as a function of distance for experiments I and II. The results given in Fig. 17(a) demonstrate the adaptation of the current bit data in accordance with the current channel conditions (e.g. the data rate is decreased in more challenging propagation conditions). This fact is corroborated by Fig. 18 that analyzes the relation between negotiated data rate and the corresponding signal strength, with lower signal strength values corresponding to higher proportions of lower modulation and coding schemes. For instance, in the region where the AUV performs the U-turn ($d \approx$ 100 m) that has more challenging propagation conditions as shown in previous sections, the rate adaptation algorithm dramatically reduces the (average) available data rate in experiments I (Fig. 17(b)) and II (Fig. 17(c)). Fig. 17(a) also demonstrates that the most favorable region for data transmission is not necessarily within short TX-RX distances and that instead the region after the *interference* zone (i.e. distances between approximately 35 and 75 m) should be considered for data offloading.

5. Discussion

In both scenarios, we attribute one of the major causes for received signal strength fluctuations are constructive or destructive interference between LOS and water-reflected paths. While in the S2S scenario, significant changes in the received signal strength are primarily induced by tides, in the S2V scenario these variations can also be attributed to varying TX-RX distances, both causing effective changes on the antenna height. This work is well aligned with previous work (e.g. [31]) that has demonstrated that minor antenna height variations can have a significant impact on the channel characteristics. Furthermore, the results provide further support to the idea that the two-ray propagation model shall accurately describe observed behavior in S2S and S2V, which will be further investigated in our future work.

Signal variations can also result from changes on the reflection surface. Regarding S2S communications, empirical results show that – despite constant antenna heights – the amplitude of the received signal varies, which is likely due to changes on the reflection surface (e.g. due to decreasing water content due to evaporation) that change the attenuation of the reflected wave. On the other hand for S2V communications, we observed that the very low AUV antenna height w.r.t. the water (comparable to the wavelength) creates situations in which the reflection is on the AUV body leading to significant signal strength variations when compared to the reflection of the secondary ray on the water.

Mobility can also impact S2V communication. We also observed divergences between both travel directions regarding RSSI magnitude and location of dips. This was particularly evident for the AP setup, in which it was possible to establish that samples acquired in the two directions come from different distributions. Also interestingly, the largest RSSI values for the *recede* direction were observed by the AP setup, and for the *approach* direction for the DMU Exp. II setup. In turn, dips in RSSI were especially evident when the vehicle was being operated manually, especially at turning points. This implies that, even when occurring at the smallest distance, turning occasions do not constitute the best intervals for data transfer between vessel and shore.

The empirical results show that the constructive/destructive interference patterns, varying reflecting surface, travel direction and particular maneuvers may have a relevant and noticeable impact on the performance of wireless communication. Equipped with such information, data volumes can be maximized – while energy efficiency is improved – by limiting data transfer to windows in which favorable conditions occur, and refraining or withholding data if such conditions are not met. Taking a step further, node mobility (e.g. AUV paths) can be planned in a way that maximizes favorable conditions, so that relevant information can be transmitted reliably and throughout a large portion of a mission. As most of the above mentioned factors are frequency-related, the system design could be further improved by considering multiple radio operating in different frequency bands.

To conclude, the following set of parameters should be *simultaneously* considered for the design and operation of WiFi S2S and S2V links, namely (*i*) tidal variations (specially for S2S communications), (*ii*) reflection surface changes (e.g. from water to AUV body or mud with varying water content), (*iii*) antenna height (e.g. higher might not be better), (*iv*) travel direction (e.g. a given travel direction might present more favorable propagation conditions), (*v*) TX-RX alignment (e.g. turning and manual operation might impair propagation conditions) and (*vi*) TX-RX separation (e.g. degraded conditions in the interference zone).

6. Conclusions

We studied the performance of short-range S2S and S2V communication links operating at 2.4 GHz under realistic conditions. The results have shown that the constructive/destructive interference patterns (e.g. resulting from tides or varying TX-RX distance), varying reflecting surface, and node mobility in all of its dimensions (e.g. turning angle) can significantly impair link quality with variations larger than 20 dB. This study provides insights into the design and operation of wireless links under these challenging operating conditions.

In future work, we further collect datasets to study the scenario in a larger number of locations and to scale for evaluating machine learning methods in this setting. For instance, we plan to further evaluate this communication link under more adverse sea conditions and consider different configurations. After performing new measurements, we shall also study the impact of the observed signal strength variations on higher network layer metrics (e.g. latency). Furthermore, we intend to continue working on modeling large and small-scale signal variation in both S2S and S2V communications. To achieve this goal, additional measurements might be required, e.g. characterize the radiation patterns of the AUV antenna set to use as input for an improved propagation model. As an end goal, we seek to provide end-users with novel and featured tools to aid the design of robust wireless communication for these links operating at near-shore scenarios.

CRediT authorship contribution statement

Pedro M. d'Orey: Conceptualization, Investigation, Methodology, Software, Writing – original draft, Writing – review & editing. **Miguel Gutiérrez Gaitán:** Investigation, Methodology, Software, Writing – original draft, Writing – review & editing. **Pedro M. Santos:** Writing – original draft, Writing – review & editing, Investigation. **Manuel Ribeiro:** Investigation, Software. **João Borges de Sousa:** Funding acquisition, Resources, Writing – original draft. **Luís Almeida:** Conceptualization, Funding acquisition, Investigation, Methodology, Writing – original draft, Writing – review & editing.

Declaration of competing interest

The authors declare the following financial interests/personal relationships which may be considered as potential competing interests: The authors report financial support was provided by the Portuguese Foundation for Science and Technology and by the European Union. Miguel Gutiérrez Gaitán reports financial support was provided by the Chilean National Agency for Research and Development.

Data availability

The Shore-to-Shore (S2S) dataset is publicly available at https://doi.org/10.17632/xyc7vv94fy.1, while the Shore-to-Vessel (S2V) dataset is available at https://doi.org/10.17632/gfxtgzp4kp.1.

Acknowledgments

References

[1] M.T. Abbas, K.-J. Grinnemo, J. Eklund, S. Alfredsson, M. Rajiullah, A. Brunstrom, G. Caso, K. Kousias, Ö. Alay, Energy-saving solutions for cellular Internet of Things: A survey, IEEE Access 10 (2022) 62073–62096.

[2] C.F. Silva, S. Ferlin, O. Alay, A. Brunstrom, B.Y. Kimura, IoT traffic offloading with multipath TCP, IEEE Commun. Mag. 59 (4) (2021) 51–57.

[3] C. Li, H. Zhang, T. Zhang, J. Rao, G. Yin, et al., Cyber-physical scheduling for predictable reliability of inter-vehicle communications, IEEE Trans. Veh. Technol. 69 (4) (2020) 4192–4206.

[4] B. Briscoe, A. Brunstrom, A. Petlund, D. Hayes, D. Ros, J. Tsang, S. Gjessing, G. Fairhurst, C. Griwodz, M. Welzl, Reducing Internet latency: A survey of techniques and their merits, IEEE Commun. Surv. Tutor. 18 (3) (2014) 2149–2196.

[5] I. Yaqoob, I.A.T. Hashem, Y. Mehmood, A. Gani, S. Mokhtar, S. Guizani, Enabling communication technologies for smart cities, IEEE Commun. Mag. 55 (1) (2017) 112–120.

[6] E. Abuhdima, J. Liu, C. Zhao, A. Elqaouaq, G. Comert, C.-T. Huang, P. Pisu, A.H. Nazeri, Impact of dust and sand on 5G communications for connected vehicles applications, IEEE J. Radio Freq. Identif. 6 (2022) 229–239.

[7] Y. Huo, X. Dong, S. Beatty, Cellular communications in ocean waves for maritime Internet of Things, IEEE Internet Things J. 7 (10) (2020) 9965–9979.

[8] A. Ijaz, L. Zhang, M. Grau, A. Mohamed, S. Vural, A.U. Quddus, M.A. Imran, C.H. Foh, R. Tafazolli, Enabling massive IoT in 5G and beyond systems: PHY radio frame design considerations, IEEE Access 4 (2016) 3322–3339.

[9] T. Zugno, F. Campagnaro, M. Zorzi, Controlling in real-time an ASV-carried ROV for quay wall and ship hull inspection through wireless links in harbor environments, in: IEEE Global Oceans, 2020, pp. 1–9.

[10] R.W. Coutinho, A. Boukerche, Towards a novel architectural design for IoT-based smart marine aquaculture, IEEE Internet of Things Mag. 5 (3) (2022) 174–179.

[11] T. Wei, W. Feng, Y. Chen, C.-X. Wang, N. Ge, J. Lu, Hybrid satellite-terrestrial communication networks for the maritime Internet of Things: Key technologies, opportunities, and challenges, IEEE Internet Things J. 8 (11) (2021) 8910–8934.

[12] T. Xia, M.M. Wang, J. Zhang, L. Wang, Maritime Internet of Things: Challenges and solutions, IEEE Wirel. Commun. 27 (2) (2020) 188–196.

[13] A. Macmillan, M.K. Marina, J.T. Triana, Slow frequency hopping for mitigating tidal fading on rural long distance over-water wireless links, in: IEEE Conference on Computer Communications Workshops, IEEE, San Diego, USA, 2010, pp. 1–5.

[14] C.-W. Ang, S. Wen, Signal strength sensitivity and its effects on routing in maritime wireless networks, in: 2008 33rd IEEE Conference on Local Computer Networks, LCN, IEEE, 2008, pp. 192–199.

[15] R. Essaadali, A. Kouki, F. Gagnon, D. Couillard, M.-E. Grandmaison, Overwater point-to-multipoint radio pathloss characterization and modeling, in: IEEE Wireless Communications and Networking Conference, WCNC, IEEE, Istanbul, Turkey, 2015, pp. 195–200.

[16] X. Liao, X. Li, Y. Wang, J. Zhou, T. Zhao, J. Zhang, Path loss modeling in urban water–land environments at 28 GHz: Considering water surface reflection and building diffraction, IEEE Antennas Wirel. Propag. Lett. 22 (4) (2022) 744–748.

[17] F.S. Alqurashi, A. Trichili, N. Saeed, B.S. Ooi, M.-S. Alouini, Maritime communications: A survey on enabling technologies, opportunities, and challenges, IEEE Internet Things J. (2022).

[18] J. Wang, H. Zhou, Y. Li, Q. Sun, Y. Wu, S. Jin, T.Q. Quek, C. Xu, Wireless channel models for maritime communications, IEEE Access 6 (2018) 68070–68088.

[19] W. Chen, C. Li, J. Yu, J. Zhang, F. Chang, A survey of maritime communications: From the wireless channel measurements and modeling perspective, Reg. Stud. Mar. Sci. 48 (2021) 102031.

[20] S. Guan, J. Wang, C. Jiang, R. Duan, Y. Ren, T.Q.S. Quek, MagicNet: The maritime giant cellular network, IEEE Commun. Mag. 59 (3) (2021) 117–123.

[21] P. Rosson, J. Estavoyer, L. Lombard, B. Miscopein, X. Popon, J.-B. Doré, D. Kténas, V. Coquen, R. Jegou-Le Bris, Long-range broadband wireless system for maritime communications in the 3.5 GHz band, in: 2021 IEEE 94th Vehicular Technology Conference (VTC2021-Fall), IEEE, 2021, pp. 1–5.

[22] X. Li, W. Feng, J. Wang, Y. Chen, N. Ge, C.-X. Wang, Enabling 5G on the ocean: A hybrid satellite-UAV-terrestrial network solution, IEEE Wirel. Commun. 27 (6) (2020) 116–121.

[23] G. Bernardi, P. Buneman, M.K. Marina, Tegola tiered mesh network testbed in rural Scotland, in: Proceedings of the 2008 ACM Wireless Networks and Systems for Developing Regions Workshop (WiNS-DR), 2008, pp. 9–16.

[24] N. Fuke, K. Sugiyama, H. Shinonaga, Long-range oversea wireless network using 2.4 GHz wireless LAN installation and performance, in: IEEE International Conference on Computer Communications and Networks (ICCN), Dallas, USA, 2003, pp. 351–356.

[25] M.G. Gaitán, P.M. d'Orey, J. Cecílio, M. Rodrigues, P.M. Santos, L. Pinto, A. Oliveira, A. Casimiro, L. Almeida, Modeling LoRa communications in estuaries for IoT environmental monitoring systems, IEEE Sens. J. 22 (21) (2022) 21312–21325.

[26] L. Parri, S. Parrino, G. Peruzzi, A. Pozzebon, Offshore LoRaWAN networking: Transmission performances analysis under different environmental conditions, IEEE Trans. Instrum. Meas. 70 (2020) 1–10.

[27] M. Pereira, Spread spectrum techniques in wireless communication part 2: Transmission issues in free space, IEEE Instrum. Meas. Mag. 13 (1) (2010) 8–14.

[28] M.G. Gaitán, P.M. Santos, L.R. Pinto, L. Almeida, Experimental evaluation of the two-ray model for near-shore WiFi-based network systems design, in: 2020 IEEE 91st Vehicular Technology Conference (VTC2020-Spring), IEEE, 2020, pp. 1–3.

[29] J. Celades-Martínez, M. Rodríguez, M.G. Gaitán, L. Almeida, Two-ray model analysis for overwater communication at 28 GHz with different heights, in: 2023 IEEE MTT-S Latin America Microwave Conference, LAMC, IEEE, 2023, pp. 144–147.

[30] A. Coelho, M. Lopes, B. Ferreira, R. Campos, M. Ricardo, Experimental evaluation of shore to unmanned surface vehicle Wi-Fi communications, in: 2018 Wireless Days, WD, IEEE, 2018, pp. 86–91.

[31] M.G. Gaitán, P.M. d'Orey, P.M. Santos, M. Ribeiro, L. Pinto, L. Almeida, J.B. De Sousa, Wireless radio link design to improve near-shore communication with surface nodes on tidal waters, in: IEEE OCEANS 2021, IEEE, San Diego, USA, 2021, pp. 1–8.

[32] K. Yang, A.F. Molisch, T. Ekman, T. Rø ste, M. Berbineau, A round earth loss model and small-scale channel properties for open-sea radio propagation, IEEE Trans. Veh. Technol. 68 (9) (2019) 8449–8460.

[33] K.S. Zaidi, V. Jeoti, M. Drieberg, A. Awang, A. Iqbal, Fading characteristics in evaporation duct: Fade Margin for a Wireless link in the South China sea, IEEE Access 6 (2018) 11038–11045.

[34] S. Aust, R.V. Prasad, I.G.M.M. Niemegeers, Outdoor long-range WLANs: A lesson for IEEE 802.11ah, IEEE Commun. Surv. Tutor. 17 (3) (2015) 1761–1775.

[35] M.G. Gaitán, L. Pinto, P.M. Santos, L. Almeida, On the two-ray model analysis for overwater links with tidal variations, in: 11º Simpósio de Informática, 2019.

[36] H. Taka, M. Wada, Tidal level estimation using a 5GHz band wireless access system, in: 2015 International Symposium on Antennas and Propagation, ISAP, IEEE, 2015, pp. 1–4.

[37] D. Taplin, Tidal Fading on Short Oversea Paths Elliptical, Vertical and Horizontal Polarisation Compared, NASA STI/Recon Technical Report N 76, 1975, p. 15328.

[38] A.D.S. Braga, H.A. Da Cruz, L.E. Eras, J.P. Araujo, M.C. Neto, D.K. Silva, G.P. Cavalcante, Radio propagation models based on machine learning using geometric parameters for a mixed city-river path, IEEE Access 8 (2020) 146395–146407.

[39] S. Surendran, M.V. Ramesh, A. Montresor, M.J. Montag, Link characterization and edge-centric predictive modeling in an ocean network, IEEE Access 11 (2023) 5031–5046.

[40] Y.-M. Le Roux, J. Ménard, C. Toquin, J.-P. Jolivet, F. Nicolas, Experimental measurements of propagation characteristics for maritime radio links, in: International Conference on Intelligent Transport Systems Telecommunications,, ITST, 2009, pp. 364–369.

[41] J.-H. Lee, J. Choi, W.-H. Lee, J.-W. Choi, S.-C. Kim, Measurement and analysis on land-to-ship offshore wireless channel in 2.4 GHz, IEEE Wirel. Commun. Lett. 6 (2) (2017) 222–225.

[42] J. Reyes-Guerrero, M. Bruno, L.A. Mariscal, A. Medouri, Buoy-to-ship experimental measurements over sea at 5.8 GHz near urban environments, in: Mediterranean Microwave Symposium, MMS, 2011, pp. 320–324.

[43] W. Hubert, Y.-M. Le Roux, M. Ney, A. Flamand, et al., Impact of ship motions on maritime radio links, Int. J. Antennas Propag. 2012 (2012).

[44] E.C. Gezer, L. Zhao, J. Beason, M. Zhou, Towards seafloor mapping using an affordable micro-UUV, in: IEEE OCEANS, IEEE, San Diego, USA, 2021, pp. 1–5.

[45] H. Zhang, S. Zhang, Y. Wang, Y. Liu, Y. Yang, T. Zhou, H. Bian, Subsea pipeline leak inspection by autonomous underwater vehicle, Appl. Ocean Res. 107 (2021) 102321.

[46] B. Yamamoto, A. Wong, P.J. Agcanas, K. Jones, D. Gaspar, R. Andrade, A.Z. Trimble, Received signal strength indication (RSSI) of 2.4 GHz and 5 GHz wireless local area network systems projected over land and sea for near-shore maritime robot operations, J. Mar. Sci. Eng. 7 (9) (2019) 290.

[47] W. Wang, G. Hoerack, T. Jost, R. Raulefs, M. Walter, U.-C. Fiebig, Propagation channel at 5.2 GHz in Baltic sea with focus on scattering phenomena, in: European Conference on Antennas and Propagation (EuCAP), IEEE, Lisbon, Portugal, 2015, pp. 1–5.

[48] E. Salahat, A. Kulaib, N. Ali, R. Shubair, Exploring symmetry in wireless propagation channels, in: European Conference on Networks and Communications (EuCNC), IEEE, Oulu, Finland, 2017, pp. 1–6.

[49] D. Pugh, P. Woodworth, Sea-Level Science: Understanding Tides, Surges, Tsunamis and Mean Sea-Level Changes, Cambridge University Press, Cambridge, United Kingdom, 2014.

[50] G. Dahman, D. Couillard, M.-E. Grandmaison, G. Poitau, F. Gagnon, Improved 2-ray model for overwater propagation channels: Modeling the instantaneous variations in the received signal strength, IEEE Wirel. Commun. Lett. 8 (3) (2019) 865–868.

[51] A. Goldsmith, Wireless Communications, Cambridge University Press, 2005.

[52] F. Van Diggelen, A-GPS: Assisted GPS, GNSS, and SBAS, in: Artech House GNSS Technology and Applications Library, Artech House, ISBN: 9781596933750, 2009.

[53] C. Specht, P. Dabrowski, J. Pawelski, M. Specht, T. Szot, Comparative analysis of positioning accuracy of GNSS receivers of Samsung Galaxy smartphones in marine dynamic measurements, Adv. Space Res. 63 (9) (2019) 3018–3028.

[54] M. Specht, Experimental Studies on the Relationship between HDOP and Position Error in the GPS System, Metrol. Meas. Syst. (2022) 17–36.

[55] M. Boban, P.M. d'Orey, Exploring the Practical Limits of Cooperative Awareness in Vehicular Communications, IEEE Trans. Veh. Technol. 65 (6) (2016) 3904–3916.

[56] G. Callebaut, L. Van der Perre, Characterization of LoRa point-to-point path loss: Measurement campaigns and modeling considering censored data, IEEE Internet Things J. 7 (3) (2019) 1910–1918.

[57] R. He, Z. Zhong, B. Ai, J. Ding, K. Guan, Analysis of the relation between Fresnel zone and path loss exponent based on two-ray model, IEEE Antennas Wirel. Propag. Lett. 11 (2012) 208–211.

[58] M.G. Gaitán, P.M. Santos, L.R. Pinto, L. Almeida, Optimal antenna-height design for improved capacity on over-water radio links affected by tides, in: Global OCEANS 2020: Singapore–US Gulf Coast, IEEE, Biloxi, MS, USA, 2020, pp. 1–7.

[59] J.-F. Quessy, F. Éthier, Cramér–von Mises and characteristic function tests for the two and k-sample problems with dependent data, Comput. Statist. Data Anal. 56 (6) (2012) 2097–2111.

[60] S. Biaz, S. Wu, Rate adaptation algorithms for IEEE 802.11 networks: A survey and comparison, in: IEEE Symposium on Computers and Communications, IEEE, Marrakech, Morocco, 2008, pp. 130–136.
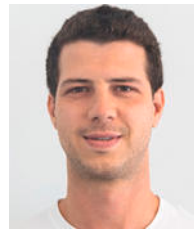
Pedro M. d'Orey received the *Licenciatura* degree in electrical and computer engineering from the University of Porto, Portugal, in 2004, the M.Sc. degree in telecommunications from Queen Mary University of London, London, U.K., in 2008, and the Ph.D. degree in telecommunications from the University of Porto, in 2014. He is currently a Research Scientist with the CISTER Research Centre in Porto, Portugal and an Invited Assistant Professor at the Faculty of Sciences of the University of Porto, Portugal. Previously, he was a Research Scientist at NEC Laboratories Europe and an R&D Engineer in the area of mobile communications. He has been involved in several European and international projects, namely within the CMU Portugal program. Four of his papers received the Best Paper Award, namely at IEEE VTC Spring and IEEE VNC 2014. His current research interests include wireless communications, automated vehicles, and AI/ML.

Miguel Gutiérrez Gaitán received his Ph.D. in electrical and computer engineering from the University of Porto, Portugal, in 2023, the M.Sc. degree in telecommunications engineering from the Politecnico di Torino, Italy, in 2009, and the B.Sc. degree in electronics engineering from the Pontificia Universidad Católica de Valparaíso, Chile, in 2007. Currently, he serves as an Assistant Professor at the Electrical Engineering Department of the Pontificia Universidad Católica de Chile, in Santiago, Chile. His research interests cover various aspects of wireless communication and networking for the Internet of Things (IoT), including channel modeling, real-time communication, and AI/ML-based network design.

Pedro M. Santos holds a full-time Researcher Fellow position at the CISTER research center, ISEP/ISEP, and he is an invited lecturer at the Faculty of Engineering of the University of Porto, Portugal. He received his Ph.D. degree in 2017 from U.Porto. Pedro has acted as P.I. in international projects, notably the Eureka MIRAI project (addressing cybersecurity) and the CMU|Portugal FLOYD project (exploring edge computing and 5G support to vehicular clients), alongside extensive participation as researcher in national and international projects relating to wireless communications and smart cities. Pedro has (co-)authored/co-authored over 40 publications in international research venues with edited proceedings or journals, and has been part of organizing committees and TPCs of well-established conferences (IEEE VNC, IEEE WFCS). His supervision service includes 2 completed Ph.D.s (with

2 on-going) and 13 M.Sc.s. Pedro received three Best Paper Awards for co-authored publications. His interests are wireless systems, 5G/6G Core and RAN, wireless positioning, vehicular communications and their interplay with autonomous driving.

Manuel Ribeiro is a versatile engineer with a Master's degree in Informatics Engineering from the University of Lisbon. Specializing in Software Engineering, his thesis, "NVL: Networked Vehicles Language", focused on coordination for multiple autonomous vehicles. Manuel's journey began in 2013 as a researcher at FEUP's Underwater Systems and Technology Laboratory, contributing to the development of the command and control framework (Neptus) and several projects related to network cooperation of autonomous heterogeneous vehicles. Manuel's expertise extends to Unmanned Aerial Vehicles, sensor integration, and aerial mapping. Recently, he transitioned to INEGI, focusing on embedded systems development.

João Borges de Sousa is an Associate Professor at the ECE Department, Porto University, and the head of the Underwater Systems and Technologies Laboratory (https://www.lsts.pt/). He holds a Ph.D. and a M.Sc. in ECE, both awarded by Porto University. His research interests include multi-domain unmanned vehicles, planning/execution control for networked vehicle systems, and applications to the ocean sciences, security, and defense. He received an outstanding teaching award from Porto University in 2008 and the IEEE Ocean Engineering Society mid-career Rising Star award in 2018. He has authored over 400 publications, including 50 journal papers.

Luís Almeida graduated from the University of Aveiro in Portugal and is currently an Associate Professor in the Electrical and Computer Engineering Department of the University of Porto, Portugal, where he coordinates the Distributed and Real-time Embedded Systems laboratory (DaRTES). He is also Vice-Director of the CISTER Research Center on Real-Time and Embedded Computing Systems, Past Chair of TCRTS - the IEEE Technical Committee on Real-Time Systems (Chair in 2020–2021) and Chair of EMSIG - the EDAA Special Interest Group on Embedded Systems. He is Editor-in-Chief of the Springer Journal of Real-Time Systems and Associate Editor of the Elsevier Journal of Systems Architecture and the SAGE International Journal on Advanced Robotic Systems. He was Program and General Chair of the IEEE Real-Time Systems Symposium in 2011 and 2012, respectively, and Local co Chair in 2016, as well as General co-Chair of CPSweek 2018. He was also Trustee of the RoboCup Federation from 2008 to 2016 and Vice-President from 2011 to 2013. He participated in numerous funded national and international research projects and regularly participates in the organization of scientific events in real-time communications for distributed industrial/embedded systems, for teams of cooperating agents and for sensor networks.